Internal Photoreference Electrode: A Powerful Characterization Method for Photoelectrochemical Quantum Dot Sensitized Solar Cells

ARTICLE *in* JOURNAL OF PHYSICAL CHEMISTRY LETTERS · APRIL 2011

Impact Factor: 7.46 · DOI: 10.1021/jz200399n

4 AUTHORS:

Idan Hod
Northwestern University
26 PUBLICATIONS **1,023** CITATIONS
SEE PROFILE

Zion Tachan
Bar Ilan University
13 PUBLICATIONS **596** CITATIONS
SEE PROFILE

Menny Shalom
Max Planck Institute of Colloids and Interfaces
37 PUBLICATIONS **1,878** CITATIONS
SEE PROFILE

Arie Zaban
Bar Ilan University
170 PUBLICATIONS **10,728** CITATIONS
SEE PROFILE

THE JOURNAL OF PHYSICAL CHEMISTRY Letters

LETTER

pubs.acs.org/JPCL

Internal Photoreference Electrode: A Powerful Characterization Method for Photoelectrochemical Quantum Dot Sensitized Solar Cells

Idan Hod, Zion Tachan, Menny Shalom, and Arie Zaban*

Chemistry Department, Bar Ilan University, Ramat Gan 52900, Israel

ABSTRACT: A unique concept of photoreference electrode developed for thin photoelectrochemical solar cells enables three-electrode characterization of quantum dot sensitized solar cells (QDSSCs) under operating conditions. Most QDSSCs utilize a polysulfide-based electrolyte, which lacks an efficient counter electrode (CE), resulting in significant performance losses. The three-electrode setup provides quantitative information regarding the potential losses associated with the CE as well as direct mapping of the effective potentials of the two cell electrodes throughout a voltage scan from open to short circuit. Moreover, the photoreference electrode method reveals a major effect of the CE quality on the recombination losses at the sensitized electrode. The method enables direct calculation of a recombination current, which arises from insufficient regeneration of the redox electrolyte by the CE. Consequently, improvement of the catalytic nature of the CE not only reduces potential losses in the photoelectrochemical cell, but it also improves the charge collection efficiency resulting in significant improvement of the overall cell performance.

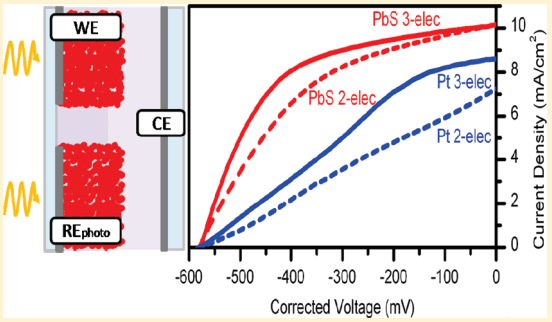

SECTION: Energy Conversion and Storage

A dye-sensitized solar cell (DSSC)[1,2] is a photoelectrochemical system that operates by photoinjection of electrons from a sensitizer molecule into a wide band gap semiconductor (usually TiO_2) where they diffuse to the external circuit, while holes are transferred to the counter electrode (CE) by the diffusion of oxidized ions in the electrolyte solution. In recent years, a large number of studies have been devoted to quantum dot sensitized solar cells (QDSSCs),[3−14] an analogue of DSSCs in which quantum dots (QDs) serve as the sensitizers. Encouraging results were obtained based on the advantages associated with the higher absorption coefficients of QDs compared with the dye sensitizers and the possibility to tailor their absorption spectra by controlling the size of the QD.[15−25] Despite the significant improvements of QDSSC performance in recent years, the maximum overall efficiencies are still lower than those of DSSCs, with record cells at around 4%.[26−28] Two major problems limit the cell efficiency: first, the lack of a suitable CE that can catalyze the redox reaction of the polysulfide (s^{2-}/s) electrolyte used in those cells;[29] second, a significant increase in the rate of several recombination paths induced by the electronic properties of the interfaces formed between the nanoporous TiO_2, QDs, and the electrolyte.[27,30−32]

In order to achieve a better understanding of the factors limiting the performance of QDSSCs, there is a need to develop a characterization method that separates the contribution of each cell component to the overall operation of the cell. Usually, the electrochemical characterization of DSSCs/QDSSCs is performed in a sandwich-type configuration, in which the sensitized working electrode (WE) is pressed against the CE to a distance of several micrometers, which is filled with the electrolyte solution.[33,34] As a result, all measurements utilizing this setup are done in a two-electrode mode, in which the applied/measured voltage of the WE is defined with respect to the CE (which also serves as a reference). Consequently, the characterization of these systems represents the whole cell without the ability to differentiate between the contributions of the WE and the CE. It is commonly assumed that the CE is catalytic enough to maintain the electrolyte potential under steady state conditions. However, under operating conditions, when high currents require significant over potentials, the CE may shift, affecting the effective potential applied/measured at the WE. Figure 1 illustrates the behavior of a photoelectrochemical solar cell during an $i-V$ scan in the two-electrode configuration, moving from open circuit (Figure 1a) toward short circuit condition (Figure 1b). At open circuit, the electrochemical potential of the system (Voc) is determined by the energy difference between the Fermi level in the TiO_2 and the CE potential, which in this case equals the electrolyte potential. However, scanning the cell potential toward short circuit, a significant potential shift of the CE may be needed in order to account for the growing photocurrent. In other words, during the scan of the WE from open to short circuit, the CE shifts from the redox potential in the opposite direction. Consequently, unlike the common perception, when the cell reaches short circuit (0 V between the two cell contacts) the potential of

Received: March 24, 2011
Accepted: April 12, 2011
Published: April 14, 2011

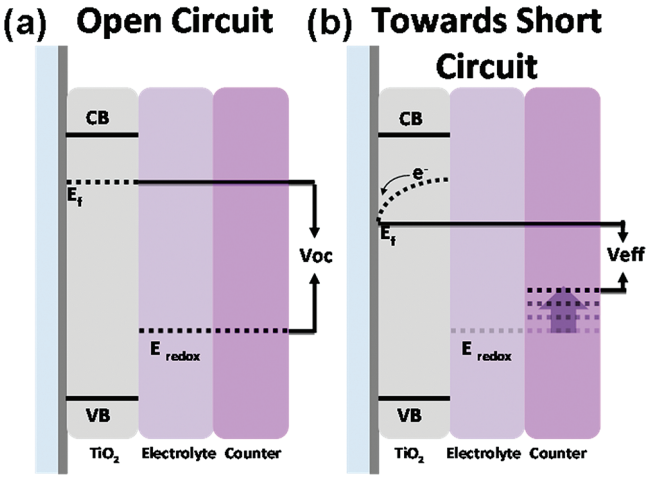

Figure 1. Illustration of the behavior of a photoelectrochemical solar cell during an $i-V$ scan in the two-electrode configuration, moving from open circuit (a) toward short circuit condition (b).

the WE is more negative than that of the redox electrolyte depending on the CE quality and the photocurrent.

Under operating conditions, the solar cell generates power via two contacts. Any shift in the CE potential leads to efficiency reduction, which is associated with the potential loss at the CE. In the same manner, $i-V$ characteristics of a solar cell provides the effective short circuit photocurrent, a value that is lower than expected for the system based on the redox potential. However, analysis of cells, mainly those utilizing ineffective CEs, requires examination of the performance of the WE solely as offered by a three-electrode measurement setup.[35] A three-electrode setup involves a reference electrode (RE) that maintains constant potential in the electrolyte solution. The voltage applied to the WE is defined with respect to the RE, while the current needed to satisfy this voltage flows through the CE regardless of any potential drops (no current is flowing through the RE). In other words, under three-electrode measurement, the potential of the WE can be scanned down to a potential equal to that of the redox electrolyte. Nevertheless, the only way to incorporate an RE into the sandwich-type cell involves significant distancing of the WE and CE, from several micrometers to the millimeter range. Moving from the thin electrolyte layer configuration to bulk electrochemistry changes critical cell operation parameters, which are characterized in this type of measurement. Consequently, a standard three-electrode configuration provides a poor presentation of a real operating cell.

Previously we demonstrated a new approach to three-electrode measurements in a standard, thin electrolyte layer, photoelectrochemical cell.[36] We replaced the typical RE by a photoelectrochemical-RE (RE_{Photo}) that is placed beside the WE, on the same glass substrate. The RE_{photo} consists of a dye-sensitized TiO_2 electrode that is maintained at open circuit conditions, thus providing constant voltage (Voc of the RE_{photo}) regardless of the reactions occurring in the adjacent cell. Practical realization of this configuration involves scraping of the front electrode through the nanoporous TiO_2 and the transparent conductive oxide to form two disconnected electrodes on a single glass substrate. Figure 2 presents a cross-section of a DSSC containing RE_{photo}. This design enables both two- and three-electrode measurements. In both cases, the measured cell is defined by the WE and the CE, which are placed on top of each

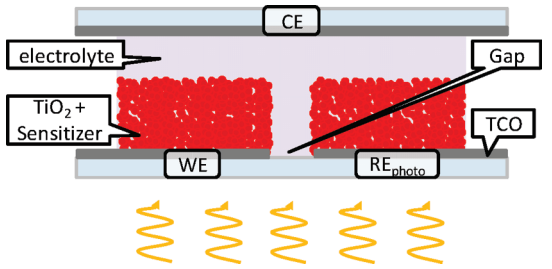

Figure 2. A cross-section of a DSSC containing RE_{photo}. This design enables both two- and three-electrode measurements. As a result, two $i-V$ characteristics of the same DSSC are available: one defining the practical performance of the cell, and one focusing on the sensitized electrode contribution without the contribution of the CE.

other in the standard sandwich configuration. The difference between the two measurement setups involves the RE knob, which is either shorted to the CE in the two-electrode measurement or connected to the RE_{photo} in the three-electrode configuration. Consequently, two $i-V$ characteristics of the same DSSC are available: one defining the practical performance of the cell, and one focusing on the sensitized electrode contribution without the contribution of the CE.

The current effort to improve the performance of QDSSCs can significantly benefit from the three-electrode setup. As mentioned above, unlike conventional DSSCs, QDSSCs suffer from a lack of optimal CE and from the presence of several recombination paths. The ability to separate between the contributions of the WEs and CEs in QDSSCs should enable clearer insight of the processes occurring in the sensitized electrode under operation. Here we present results showing the effect of the CE quality on the performance of CdSe-QDSSCs. First, the internal RE_{photo} concept is demonstrated using three Pt CEs, which differ by their catalytic qualities in a standard DSSC. Second, we compare the operation of Pt and PbS[37] CEs in the polysulfide-based CdSe-QDSSC, quantifying the voltage drops associated with each CE. Finally, we demonstrate the effect of the CE quality on the recombination processes occurring at the sensitized electrode utilizing direct calculation of the recombination current resulting from lower CE quality.

Figure 3 demonstrates the significance of the RE_{photo}-based three-electrode measurement of photoelectrochemical solar cells. The $i-V$ characteristics of a conventional DSSC were measured using three Pt CEs that differ by their catalytic qualities (achieved by a gentle scraping of the electrode surface). For each CE, two $i-V$ curves were measured: one in the two-electrode setup and one in the three-electrode setup. The only technical difference between the two measurements is the external connection of the RE knob to the cell. The two-electrode-based curves are presented in Figure 3a with the standard potential scale. By contrast, the three-electrode measurements presented in Figure 3b share a voltage scale that is shifted by the RE_{photo} potential, i.e., Voc. Figure 3c shows both the two- (dashed lines) and the three-electrode (solid lines) measurements on a common potential scale, in which the three-electrode plots were shifted by Voc (zero current potentials match). For the high-quality CE, there is hardly any difference between the two- and three-electrode measurements. However, decline in the qualities of the CEs results in growing differences: the three-electrode setup exhibits higher photocurrents and fill factors compared to the corresponding two-electrode measurements. Two factors

dx.doi.org/10.1021/jz200399n |J. Phys. Chem. Lett. 2011, 2, 1032–1037

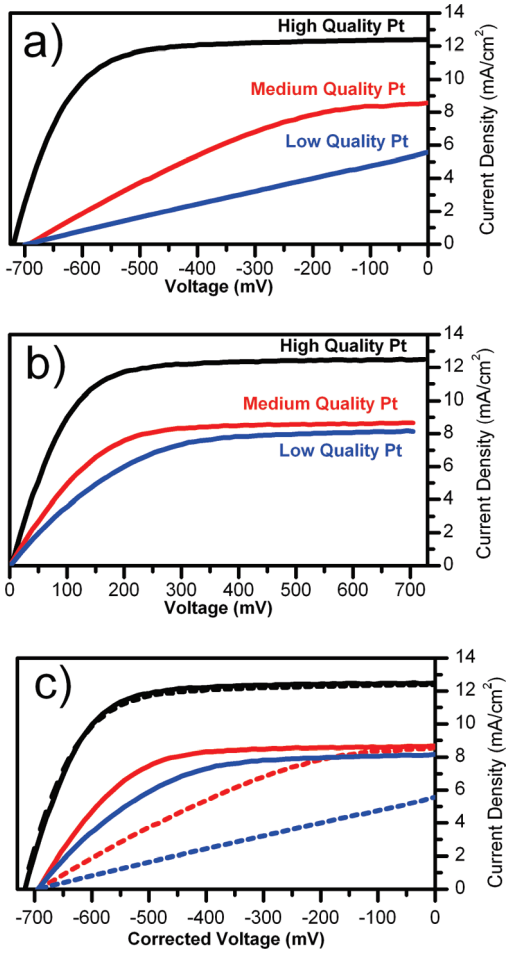

Figure 3. $i-V$ characteristics of a conventional DSSC, measured using three Pt CEs that differ by their catalytic qualities. (a) Two-electrode-based curves under standard potential scale. (b) Three-electrode-based curves, which share a voltage scale that is shifted by the RE_{photo} potential, i.e., Voc. (c) Both the two- (dashed lines) and the three-electrode (solid lines) measurements on a common potential scale, in which the three-electrode plots were shifted by Voc (zero current potentials match). Black curves: high-quality Pt; red curves: medium-quality Pt; and blue curves: low-quality Pt.

associated with the three-electrode setup are responsible for the higher photocurrent and fill factor values: (i) The resistances associated with the charge transfer processes at the CE are eliminated in the three-electrode measurement. (ii) The potential of the WE is defined with respect to the redox rather than that of the CE, which shifts positively as the photocurrent increases.

While the resistances associated with the CE and the resulting potential drops are important parameters, the three-electrode measurements reveal a critical effect of the CE quality on the recombination processes in the cell. In standard three-electrode electrochemistry, within reasonable limits the quality of the CE has no effect on the $i-V$ characteristics of a cell. As long as the system can provide the compliance voltage, the cell current is solely defined by the WE potential. Under these considerations, one would expect the photocurrents of the three cells presented in Figure 3b to be similar, regardless of the CE quality. However, this is not the case for photoelectrochemical solar cells that involve recombination processes. Despite the similar potential of the three WEs presented in Figure 3b, the photocurrents

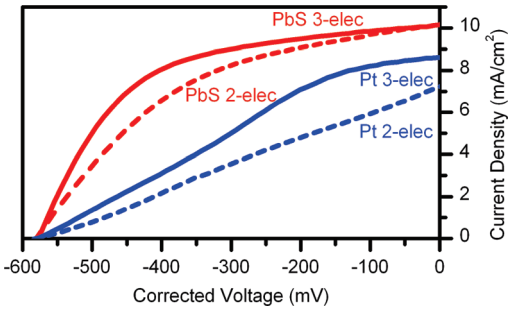

Figure 4. $i-V$ curves of a CdSe-QD-sensitized WE measured with two CEs. The red curves were measured with the PbS CE using the two- and three-electrode setups (dashed and solid lines, respectively). In a similar way, the blue curves represent the measurements utilizing the Pt electrode.

decrease with declining CE quality, indicating higher recombination loss currents. In other words, poorer CE quality lowers the collection efficiency of the hole-carrying ions, thus increasing the recombination rates in the cell which finally results in lower photocurrents.

As shown in Figure 3c, the significance of the three-electrode setup increases for cells that lack high-quality CEs, which is the case of most QDSSCs. Utilizing polysulfide electrolytes, QDSSCs suffer from low catalytic activity of many optional CEs including Pt.[29] Recently we showed that PbS-based CEs significantly improve the performance of such QDSSCs in comparison with the common CE options.[37] In the following, we utilize QDSSCs to demonstrate the importance of the RE_{photo}, demonstrating the new insights available by the three-electrode measurement.

Figure 4 presents the $i-V$ curves of a CdSe-QD-sensitized WE measured with two CEs. The red curves were measured with the PbS CE using the two- and three-electrode setups (dashed and solid lines, respectively). In a similar way, the blue curves represent the measurement utilizing the Pt electrode. The common practice of comparing the two-electrode measurements shows that the PbS CE is superior to Pt with respect to the photocurrent and fill factor values. However, direct quantitative evidence of the source for the PbS superiority, e.g., better catalytic activity and/or lower sheet resistance, requires analysis of the three-electrode measurements.

The three-electrode setup measures the photocurrent in the cell as a function of the sensitized WE potential while the two-electrode setup measures the photocurrent with respect to the cell potential (including drops at the CE). For any given photocurrent, the difference in voltage between the two- and three-electrode measurements equals the potential drop across the CE. Consequently, simple calculation utilizing the two- and three-electrode curves enables quantitative description of the potential distribution in the cell as a function of the operating cell voltage; the results are shown in Figure 5.

Figure 5 plots the potentials of both the CE and the TiO_2 WE versus the redox electrolyte, during the cell scan from open to short circuit (Figure 5a for the Pt CE based cell and Figure 5b for the PbS CE). In an optimal cell where the drop at the CE is negligible, the WE potential equals that of the whole cell, while the CE potential with respect to that of the redox couple is practically zero throughout the scan. However, for less catalytic CEs, such as the ones presented in Figure 5, a scan from open to short circuit involves a growing need for reduction power, which

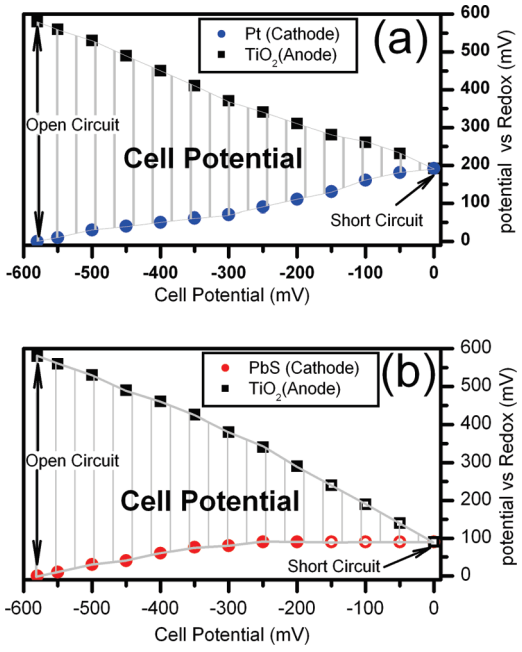

Figure 5. A plot of the potentials of both the CE and the TiO_2 WE versus the redox electrolyte, during the cell scan from open to short circuit. (a) Pt CE-based cell. The over potential lost at the CE increases steadily from 0 to 200 mV during the scan from open to short circuit. (b) PbS CE-based cell. The negative shift of the CE potential is less significant reaching 100 mV at short circuit despite the higher currents generated by this cell. Hollow symbols mark evaluated values coming from large error bars as a result of small differences in photocurrents measured using two- and three-electrode setups.

results in an increasing negative shift of the CE potential. In the case of the Pt CE (Figure 5a), the overpotential lost at the CE increases steadily from 0 to 200 mV during the scan from open to short circuit. In other words, the actual potential of the WE with respect to the electrolyte is higher than the voltage measured between the two cell contacts. When this cell is set to short circuit (0 V between the two contacts), the actual potential of both the sensitized anode (WE) and the Pt cathode (CE) is 200 mV above the potential of the redox electrolyte. Replacing the Pt with the more catalytic PbS CE results in smaller deviation from optimal behavior (Figure 5b). The negative shift of the CE potential is less significant, reaching 100 mV at short circuit despite the higher currents generated by this cell.

Further toward the evaluation of the effective potentials in the cell, the three-electrode measurement enables a comparison of the two cells under a common potential scale. The two three-electrode measurements presented in Figure 4 provide the photocurrents of the Pt- and PbS-based cells, both with respect to the sensitized anode (WE) potential (vs the redox electrolyte). Despite the similar energetic position of the two WEs, the photocurrent of the Pt containing cell is significantly lower throughout the voltage scan. As discussed above, the two three-electrode measurements of the sensitized WE should not be affected by the nature of the CE unless the associated catalytic quality affects the recombination loss rates. Apparently, the poorer catalytic quality of the Pt CE slows the redox regeneration process, thus affecting the concentration gradients in the electrolyte. Compared with the PbS-based cell, the diffusion of the hole carrying ions toward the Pt CE is slower, and their concentration in the nanoporous

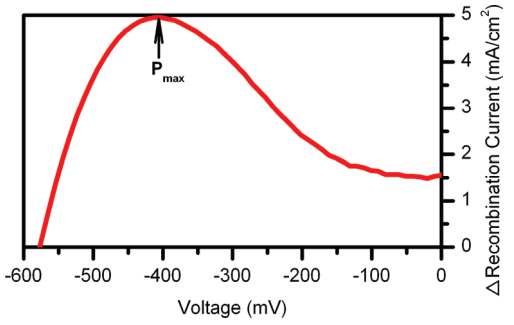

Figure 6. Recombination current difference associated with the replacement of the PbS by the Pt CE, demonstrating the important role played by the CE in the recombination process. The calculation was done by the subtraction of the three-electrode $i-V$ curves measured with PbS and Pt CEs.

electrode is higher, resulting in faster reaction with the photoinjected electrons. Since recombination is the only possible source for the difference between the two three-electrode measurements of Figure 4, a simple subtraction of the curves provides the recombination current difference associated with the replacement of the PbS by the Pt CE. The calculation presented in Figure 6 demonstrates the important role played by the CE in the recombination process. The recombination current difference starts at 1.5 mA/cm^2 at 0 V, reaching a value as high as 5 mA/cm^2 around the maximum power point of the PbS CE-based cell. We note that Figure 6 does not represent the total recombination current in the cell but rather only the losses resulting from the CE quality. However, it shows that the CE affects the cell performance beyond the issues related to potential drops at the CE.

The use of an internal RE_{photo} is proven to be an efficient and powerful tool for the characterization of photoelectrochemical solar cells under regular working conditions. We have shown that this tool is especially beneficial when applied to systems that suffer from a lack of optimal CE, such as QDSSCs, enabling direct measurement of the WE operation and the influence of the CE on the whole cell.

The quality of the CE could be assessed by comparing between an $i-V$ curve measured in two- and three-electrode setup, which reveals the voltage drops across the CE throughout the voltage scan. In addition, one can obtain detailed insight regarding the recombination processes in the studied system by comparing three-electrode measurements that utilize different CEs.

EXPERIMENTAL SECTION

TiO_2 Electrode Preparation. Fluorine-doped tin oxide (FTO) was purchased from Pilkington (TEC 8) with 8 ohm/square sheet resistance. Commercial TiO_2 paste provided by Solaronix (Switzerland) was spread by doctor blade technique. All electrodes were sintered at 450 °C for 30 min. The thickness of the electrodes was 5 μm measured by the profilometer (Surftest SV-500).

DSSC Preparation. The dye (*cis*-di(isothiocyanato)-*N*-bis(4,4′-dicarboxy-2,2′-bipyridine) ruthenium(II)) was adsorbed by immersing the TiO_2 electrodes overnight in a 0.5 mM ethanol solution of the dye. As a CE, we used a Pt-coated F-doped SnO_2 film.

0.5 M LiI/0.05 M I2 in 1:1 acetonitrile:3-methyl-2-oxazolidinone (NMO) was used as an electrolyte.

CdSe QD Deposition. A seeding layer of CdS QD was deposited prior to the CdSe deposition by four cycles of the Silar method.[38] All electrodes were sensitized with CdSe QDs grown by chemical

dx.doi.org/10.1021/jz200399n |J. Phys. Chem. Lett. 2011, 2, 1032–1037

bath deposition (CBD) following the procedure published by Gorer and Hodes.[39] First, as the Se source, an 80 mM sodium selenosulphate (Na_2SeSO_3) solution was prepared by dissolving elemental Se powder in a 200 mM Na_2SO_3 solution. Second, 80 mM $CdSO_4$ and 120 mM trisodiumsalt of nitrilotriacetic acid ($N(CH_2COONa)_3$) were mixed in a volume ratio of 1:1. Finally, both solutions were mixed in a volume ratio of 1:2. The mesoporous TiO_2 electrodes were placed in a glass container filled with the final solution for 24 h deposition time at 10 °C under dark. The as-sensitized electrodes were coated with ZnS by alternately dipping into 0.1 M $Zn(CH_3COO)_2$ and 0.1 M Na_2S solutions for 1 min/dip, rinsing with deionized water between each dip (two cycles overall).[22]

An aqueous polysulfide electrolyte was prepared, consisting of 1 M sodium sulfide (Na_2S), 0.1 M sulfur (S), and 0.1 M sodium hydroxide (NaOH) solution in deionized water. A Pt-coated conducting FTO glass served as a CE. PbS CE was prepared by pretreating a Pb metal foil (Alfa Aesar), reported elsewhere.[37]

Solar Cell Configuration. A sandwich cell configuration was used to measure the performance of all the cells. A narrow insulating gap (approximately 1 mm thick) was made across the electrode using a fine ceramic glass scraper. The gap resistance was higher than 100 MΩ/square.

Optical and Electrical Characterization. Current−potential ($i-V$) measurements were performed with an Eco-Chemie Potentiostat with a scan rate of 10 mV/s. A 250 W xenon arc lamp (Oriel) calibrated to 100 mW/cm2 served as a light source. The illuminated area of the cell was 0.45 cm^2.

AUTHOR INFORMATION

Corresponding Author

*E-mail address: zabana@mail.biu.ac.il.

ACKNOWLEDGMENT

This research was supported by The Israel Science Foundation.

REFERENCES

(1) Gratzel, M. J. Dye-Sensitized Solar Cells. *Photochem. Photobiol. C: Photochem. Rev.* **2003**, *4*, 145–153.

(2) Hodes, G.; Howell, I. D. J.; Peter, L. M. Nanocrystalline Photoelectrochemical Cells - A New Concept in Photovoltaic Cells. *J. Electrochem. Soc.* **1992**, *139*, 3136–3140.

(3) Baker, D. R.; Kamat, P. V. Photosensitization of TiO_2 Nanostructures with CdS Quantum Dots: Particulate versus Tubular Support Architectures. *Adv. Funct. Mater.* **2009**, *19*, 805–811.

(4) Diguna, L. J.; Shen, Q.; Kobayashi, J.; Toyoda, T. High Efficiency of CdSe Quantum-Dot-Sensitized TiO_2 Inverse Opal Solar Cells. *Appl. Phys. Lett.* **2007**, *91*, 023116.

(5) Farrow, B.; Kamat, P. V. CdSe Quantum Dot Sensitized Solar Cells. Shuttling Electrons Through Stacked Carbon Nanocups. *J. Am. Chem. Soc.* **2009**, *131*, 11124–11131.

(6) Gur, I.; Fromer, N. A.; Geier, M. L.; Alivisatos, A. P. Air-Stable All-Inorganic Nanocrystal Solar Cells Processed from Solution. *Science* **2005**, *310*, 462–465.

(7) Hodes, G. Comparison of Dye- and Semiconductor-Sensitized Porous Nanocrystalline Liquid Junction Solar Cells. *J. Phys. Chem. C* **2008**, *112*, 17778–17787.

(8) Kamat, P. V. Meeting the Clean Energy Demand: Nanostructure Architectures for Solar Energy Conversion. *J. Phys. Chem. C* **2007**, *111*, 2834–2860.

(9) Kamat, P. V. Quantum Dot Solar Cells. Semiconductor Nanocrystals as Light Harvesters. *J. Phys. Chem. C* **2008**, *112*, 18737–18753.

(10) Loef, R.; Houtepen, A. J.; Talgorn, E.; Schoonman, J.; Goossens, A. Study of Electronic Defects in CdSe Quantum Dots and Their Involvement in Quantum Dot Solar Cells. *Nano Lett.* **2009**, *9*, 856–859.

(11) Ruhle, S.; Shalom, M.; Zaban, A. Quantum-Dot-Sensitized Solar Cells. *ChemPhysChem* **2010**, *11*, 2290–2304.

(12) Vogel, R.; Hoyer, P.; Weller, H. Quantum-Sized PbS, CdS, Ag_2S, Sb_2S_3, and Bi_2S_3 Particles as Sensitizers for Various Nanoporous Wide-Bandgap Semiconductors. *J. Phys. Chem.* **1994**, *98*, 3183–3188.

(13) Hossain, A.; Yang, G. W.; Parameswaran, M.; Jennings, J. R.; Wang, Q. Mesoporous SnO_2 Spheres Synthesized by Electrochemical Anodization and Their Application in CdSe-Sensitized Solar Cells. *J. Phys. Chem. C* **2010**, *114*, 21878–21884.

(14) Zhu, G.; Cheng, Z.; Lv, T.; Pan, L.; Zhao, Q.; Sun, Z. Zn-Doped Nanocrystalline TiO_2 Films for CdS Quantum Dot Sensitized Solar Cells. *Nanoscale* **2010**, *2*, 1229–1232.

(15) Berea, E. M.; Shalom, M.; Gimenez, S.; Hod, I.; Mora-Sero, I.; Zaban, A.; Bisquert, J. Design of Injection and Recombination in Quantum Dot Sensitized Solar Cells. *J. Am. Chem. Soc.* **2010**, *132*, 6834–6839.

(16) Buhbut, S.; Itzhakov, S.; Tauber, E.; Shalom, M.; Hod, I.; Geiger, T.; Garini, Y.; Oron, D.; Zaban, A. Built-in Quantum Dot Antennas in Dye-Sensitized Solar Cells. *ACS Nano* **2010**, *4*, 1293–1298.

(17) Giménez, S.; Mora-Seró, I.; Macor, L.; Guijarro, N.; Lana-Villarreal, T.; Gómez, R.; Diguna, L. J.; Shen, Q.; Toyoda, T.; Bisquert, J. Improving the Performance of Colloidal Quantum-Dot-Sensitized Solar Cells. *Nanotechnology* **2009**, *20*, 295204.

(18) Pattantyus-Abraham, A. G.; Kramer, I. J.; Barkhouse, A. R.; Wang, X. H.; Konstantatos, G.; Debnath, R.; Levina, L.; Raabe, I.; Nazeeruddin, M. K.; Gratzel, M.;Depleted-Heterojunction Colloidal Quantum Dot Solar Cells. *ACS Nano* **2010**, *4*, 3374–3380.

(19) Shalom, M.; Albero, J.; Tachan, Z.; Martinez-Ferrero, E.; Zaban, A.; Palomares, E. Quantum Dot-Dye Bilayer-Sensitized Solar Cells: Breaking the Limits Imposed by the Low Absorbance of Dye Monolayers. *J. Phys. Chem. Lett.* **2010**, *1*, 1134–1138.

(20) Shalom, M.; Dor, S.; Ruhle, S.; Grinis, L.; Zaban, A. Core/CdS Quantum Dot/Shell Mesoporous Solar Cells with Improved Stability and Efficiency Using an Amorphous TiO_2 Coating. *J. Phys. Chem. C* **2009**, *113*, 3895–3898.

(21) Shalom, M.; Ruhle, S.; Hod, I.; Yahav, S.; Zaban, A. Energy Level Alignment in CdS Quantum Dot Sensitized Solar Cells Using Molecular Dipoles. *J. Am. Chem. Soc.* **2009**, *131*, 9876.

(22) Shen, Q.; Kobayashi, J.; Diguna, L. J.; Toyoda, T. Effect of ZnS Coating on the Photovoltaic Properties of CdSe Quantum Dot-Sensitized Solar Cells. *J. Appl. Phys.* **2008**, *103*, 084304.

(23) Yu, Y. H.; Kamat, P. V.; Kuno, M. A CdSe Nanowire/Quantum Dot Hybrid Architecture for Improving Solar Cell Performance. *Adv. Funct. Mater.* **2010**, *20*, 1464–1472.

(24) Zhao, N.; Osedach, T. P.; Chang, L. Y.; Geyer, S. M.; Wanger, D.; Binda, M. T.; Arango, A. C.; Bawendi, M. G.; Bulovic, V. Colloidal PbS Quantum Dot Solar Cells with High Fill Factor. *ACS Nano* **2010**, *4*, 3743–3752.

(25) Salant, A.; Shalom, M.; Hod, I.; Faust, A.; Zaban, A.; Banin, U. Quantum Dot Sensitized Solar Cells with Improved Efficiency Prepared Using Electrophoretic Deposition. *ACS Nano* **2010**, *4*, 5962–5968.

(26) Lee, H.; Wang, M.; Chen, P.; Gamelin, D. R.; Zakeeruddin, S. M.; Gratzel, M.; Nazeeruddin, M. K. Efficient CdSe Quantum Dot-Sensitized Solar Cells Prepared by an Improved Successive Ionic Layer Adsorption and Reaction Process. *Nano Lett.* **2009**, *9*, 4221–4227.

(27) Gonzalez-Pedro, V.; Xu, X. Q.; Mora-Sero, I.; Bisquert, J. Modeling High-Efficiency Quantum Dot Sensitized Solar Cells. *ACS Nano* **2010**, *4*, 5783–5790.

(28) Huang, S.; Zhang, Q.; Huang, X.; Guo, X.; Deng, M.; Li, D.; Luo, Y.; Shen, Q.; Toyoda, T.; Meng, Q. Fibrous CdS/CdSe Quantum Dot Co-sensitized Solar Cells Based on Ordered TiO_2 Nanotube Arrays. *Nanotechnology* **2010**, *21*, 375201.

(29) Hodes, G.; Manassen, J.; Cahen, D. Electrocatalytic Electrodes for the Polysulfide Redox System. *J. Electrochem. Soc.* **1980**, *127*, 544–549.

(30) Mora-Sero, I.; Bisquert, J. Breakthroughs in the Development of Semiconductor-Sensitized Solar Cells. *J. Phys. Chem. Lett.* **2010**, *1*, 3046–3052.

(31) Zhu, H. M.; Song, N. H.; Lian, T. Q. Controlling Charge Separation and Recombination Rates in CdSe/ZnS Type I Core−Shell Quantum Dots by Shell Thicknesses. *J. Am. Chem. Soc.* **2010**, *132*, 15038–15045.

(32) Jin, S. Y.; Lian, T. Q. Electron Transfer Dynamics from Single CdSe/ZnS Quantum Dots to TiO_2 Nanoparticles. *Nano Lett.* **2009**, *9*, 2448–2454.

(33) Cahen, D.; Hodes, G.; Gratzel, M.; Guillemoles, J. F.; Riess, I. Nature of Photovoltaic Action in Dye-Sensitized Solar Cells. *J. Phys. Chem. B* **2000**, *104*, 2053–2059.

(34) Gratzel, M. Perspectives for Dye-Sensitized Nanocrystalline Solar Cells. *Prog. Photovoltaics* **2000**, *8*, 171–185.

(35) Yan, S. G.; Hupp, J. T. Energetics of Electron Transfer at the Nanocrystalline Titanium Dioxide Semiconductor/Aqueous Solution Interface: pH Invariance of the Metal-Based Formal Potential of a Representative Surface-Attached Dye Couple. *J. Phys. Chem. B* **1997**, *101*, 1493–1495.

(36) Zaban, A.; Zhang, J.; Diamant, Y.; Melemed, O.; Bisquert, J. Internal Reference Electrode in Dye Sensitized Solar Cells for Three-Electrode Electrochemical Characterizations. *J. Phys. Chem. B* **2003**, *107*, 6022–6025.

(37) Tachan, Z.; Shalom, M.; Hod, I.; Ruhle, S.; Tirosh, S.; Zaban, A. PbS as a Highly Catalytic Counter Electrode for Polysulfide-Based Quantum Dot Solar Cells. *J. Phys. Chem. C* **2011**, *115*, 6162–6166.

(38) Vogel, R.; Pohl, K.; Weller, H. Sensitization of Highly Porous, Polycrystalline TiO_2 Electrodes by Quantum Sized Cds. *Chem. Phys. Lett.* **1990**, *174*, 241–246.

(39) Gorer, S.; Hodes, G. Quantum-Size Effects in the Study of Chemical Solution Deposition Mechanisms of Semiconductor-Films. *J. Phys. Chem.* **1994**, *98*, 5338–5346.